Bulletin of the Seismological Society of America, Vol. 92, No. 2, pp. 581–589, March 2002

Active Tectonics of Northeastern Sonora, Mexico (Southern Basin and Range Province) and the 3 May 1887 M_w 7.4 Earthquake

by Max Suter and Juan Contreras

Abstract North–south-striking and west-dipping Basin and Range province normal faults form the western edge of the Sierra Madre Occidental plateau in northeastern Sonora. These faults and associated half-grabens extend over a distance of more than 300 km between the San Bernardino basin in the north and the Sahuaripa basin in the south. An earthquake in 1887 ruptured three neighboring segments of this major fault zone. Our field mapping in this region indicates that the surface rupture of the 1887 earthquake extends farther to the south and is considerably longer (101.4 km end-to-end length) than previously reported. A compilation of the seismicity in the epicentral region of the 1887 earthquake shows the epicenters to be distributed in well-defined clusters at the northern end of the 1887 surface rupture, in the step-overs between the three rupture segments, on a neighboring fault in the west (Fronteras fault), and on fault segments farther south along the same fault zone (Granados region). The distribution of seismicity correlates well with calculated changes in Coulomb failure stress resulting from the 1887 earthquake.

Introduction

Most of northern Mexico belongs tectonically and morphologically to the southern Basin and Range province. This large-scale pattern of roughly north–south-striking high-angle normal faults reaches practically from coast to coast (see distribution of fault traces compiled by Stewart *et al.* [1998] and the digital elevation model shown in Fig. 1). There are indications that this deformation is still active. Major historical earthquakes have occurred in this region, such as the 1887 Bavispe, Sonora (M_w 7.4) (Natali and Sbar, 1982), the 1928 Parral, Chihuahua (M_w 6.5) (Doser and Rodríguez, 1993), and the 1931 Valentine, Texas (M_w 6.4) (Doser, 1987) events (Fig. 1), and from borehole elongations, it can be inferred that the least horizontal stress is oriented approximately east–west, perpendicular to the traces of Basin and Range province faults (Suter, 1991). However, we do not know the bulk strain of this area nor how the deformation is distributed in space and time. The present-day east–west extension rate is less than 6 mm/yr in the northern Basin and Range, between the Wasatch fault and the Sierra Nevada block (Dixon *et al.,* 2000), but is unknown for the Mexican Basin and Range, where the available knowledge base is limited to a few regional studies of late Cenozoic extension (e.g., Nieto-Samaniego *et al.,* 1999; Henry and Aranda-Gómez, 2000), regional seismicity studies (e.g., Doser and Rodríguez, 1993), and directional data of stress (Suter, 1987, 1991).

In this study, we present the rupture parameters of a major historical earthquake that occurred in this region in 1887. This rupture reactivated parts of a fault zone, more than 300 km long, along the western margin of the Sierra Madre Occidental plateau. We also present a compilation of the seismicity in northeastern Sonora. The distribution of seismicity is graphed on contour and shaded relief maps to obtain a better resolution of the Basin and Range fault pattern of northeastern Sonora and to identify seismically active fault segments. Furthermore, we present a model of the change in static Coulomb failure stress resulting from the rupture of the 1887 earthquake and evaluate, based on our model, to what extent the distribution of seismicity may be controlled by the calculated stress changes. Finally, we discuss the overall neotectonic setting of this fault zone.

Surface Rupture of the 3 May 1887 Earthquake

This earthquake ruptured three major range-bounding normal faults. The surface rupture (Fig. 2) extends farther to the south than previously reported. The rupture dips ~74° W and is composed (from south to north) of the (1) Otates (length l = 18.9 km, maximum vertical separation a = 220 cm, average vertical separation b = 152 cm), (2) Teras (l = 20.7 km, a = 184 cm, b = 112 cm), and (3) Pitáycachi (l = 43.8 km, a = 487 cm, b = 232 cm) segments. The existence of the previously unreported Otates segment explains why the damage was most severe in Bavispe and Villa Hidalgo (formerly Óputo), which are located closer to this segment than to the previously known segments (Fig. 2). The limits between the defined rupture segments are character-

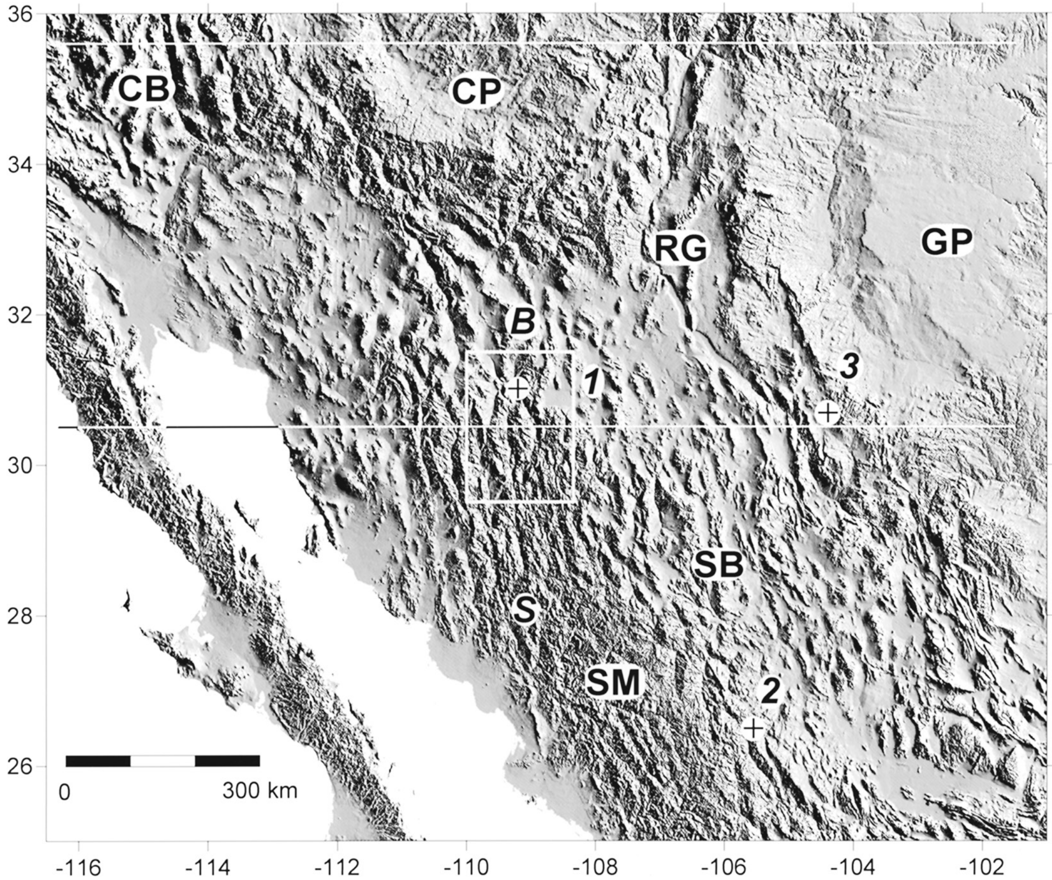

Figure 1. Digital elevation model (GTOPO30, 30 arc-sec resolution) of southwestern North America with morphological–neotectonic provinces (CB, central Basin and Range; CP, Colorado plateau; RG, Río Grande rift; GP, Great Plains; SB, southern Basin and Range; SM, Sierra Madre Occidental plateau). B, San Bernardino basin; S, Sahuaripa basin. Crosses indicate the epicenters of the (1) 1887 Sonora (M_w 7.4), (2) 1928 Parral (M_w 6.5), and (3) 1931 Valentine (M_w 6.4) earthquakes. Box: region covered by Figure 2 and approximate location of study area. The lines across the Basin and Range trend are the traces of the topographic sections in Figure 4.

ized by structural discontinuities (step-overs) and minima in the displacement distribution, which suggests that the segments ruptured independently and did not merge at depth. Macroseismic observations (Aguilera, 1888) also indicate that this was a composite earthquake with the individual shocks separated only by a few seconds. Segmentation of the surface rupture exists on a smaller scale but is not reflected in the slip distribution (dePolo *et al.,* 1991). Including two isolated minor segments to the north of the Pitáycachi segment (Fig. 2), the known rupture trace length adds now up to 86.3 km, and the distance between the rupture trace extremities is 101.4 km. The rupture trace extremities are located at 109.149° W/31.270° N in the north and 109.165° W/30.356° N in the south. Based on the end-to-end length of the rupture trace and the length versus magnitude regression by Wells and Coppersmith (1994), M_w is estimated as 7.4 $\pm$ 0.3. The surface rupture of the Pitáycachi segment has a well-developed branching pattern (five north-facing bifurcations in the northern part of the segment, two south-facing bifurcations in its southern part), which suggests that the rupture of the Pitáycachi segment initiated in its central part where the polarity of the rupture bifurcations changes. The rupture is characterized by east–west extension, perpendicular to the fault trace. However, deflected stream channels and a left-stepping en-echelon rupture array indicate locally a right-lateral strike-slip component in the central part of the Pitáycachi segment. A more detailed structural analysis of the surface rupture of this earthquake is in preparation.

Basin and Range Province Faults

The Basin and Range fault pattern of this region is shown in Figure 2; the traces of major faults are based on the compilation by Fernández-Aguirre *et al.* (1993) and fieldwork performed in this study. Elevations seen in Figure 2 range between 400 and 2600 m. Spacing between major faults is about 30 km, and the basins are about 10 km wide. In cross section, the faults form a staircase series of half-

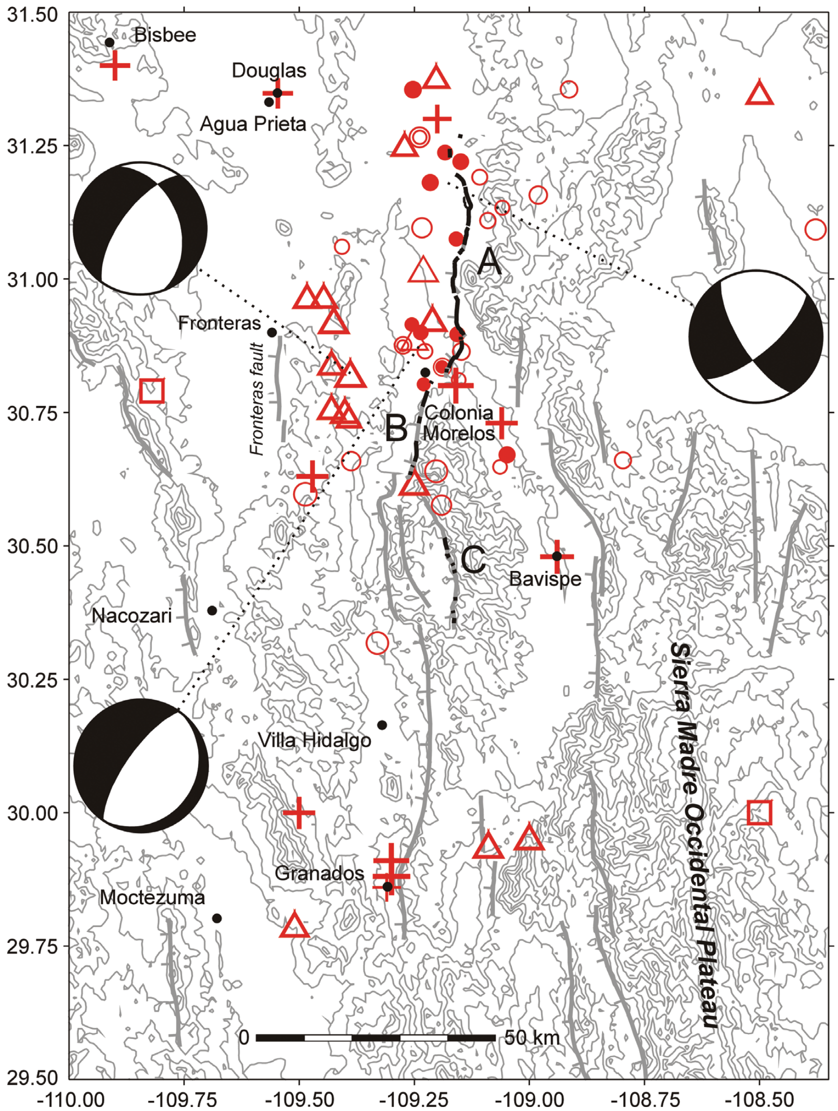

Figure 2. Seismotectonic map of northeastern Sonora (location marked in Fig. 1) with earthquake epicenters, the 1887 rupture trace (in black; A, Pitáycachi segment; B, Teras segment; C, Otates segment), focal mechanisms, and the interpreted traces of major Basin and Range faults (in gray). Epicenter symbols: cross, location based on intensity distribution; triangle, located instrumentally, magnitude specified; square, located instrumentally, magnitude unspecified; circle, microearthquake (closed circle: high quality; open circle: low quality). The symbol sizes are proportional to the magnitude (or maximum intensity) of the events. The topography has a 200-m contour interval.

grabens, with most of the graben-bounding faults dipping toward the west. These faults define the western edge of the less-deformed Sierra Madre Occidental plateau (Figs. 1 and 2). Along strike, these faults and associated half-grabens extend over a distance of more than 300 km, between the Sahuaripa basin in the south and the San Bernardino basin in the north (Fig. 1).

The three major rupture segments of the 1887 earthquake coincide with three of these north–south-striking and west-dipping Basin and Range faults and associated half-grabens (Fig. 2). The maximum throw is at least 1360 m for the Otates fault and at least 1640 m for the Teras fault with respect to the base of the basalt sequence overlying the ignimbrites of the Sierra Madre Occidental volcanic province. This stratigraphic marker can be correlated between the hanging-wall and footwall blocks of these two faults. In the case of the Pitáycachi fault, the throw (4080 m) can be estimated by adding the height of Cerro Pitáycachi above the alluvial fan surface (1080 m) to the thickness of the San Bernardino basin fill close to the fault (~3000 m), estimated by Sumner (1977) based on gravimetric measurements and modeling. The dip of these faults at the surface is approximately 74°. From the age of basalt flows intercalated with the lowermost fill of nearby basins (Gans, 1997; McDowell *et al.,* 1997; González León *et al.,* 2000), it can be inferred that Basin and Range faulting in the epicentral region of the 1887 earthquake started ca. 23 Ma (Miocene).

Assuming a 23 m.y. duration of fault activity and a dip of 74°, the net geologic slip rates are at least 0.07 mm/yr for the Teras fault, at least 0.06 mm/yr for the Otates fault, and ca. 0.18 mm/yr for the Pitáycachi fault. On the other hand, the Quaternary slip rate of the Pitáycachi fault, obtained from the fault scarp morphology and the estimated age of soils formed on alluvial surfaces displaced by the fault, is only 0.015 mm/yr (Bull and Pearthree, 1988; Pearthree *et al.,* 1990), 12 times slower than its long-term rate. Such a decrease in slip rate with time is also characteristic for many faults of the Río Grande rift; the Socorro fault zone, for example, slowed from 0.18–0.20 mm/yr in the latest Miocene to about 0.05 mm/yr in the Pliocene and 0.02–0.04 mm/yr in the past 0.75 Ma (Machette, 1998).

The Quaternary slip rates of the Teras and Otates faults are likely to be higher than the slip rate of the Pitáycachi fault because the range fronts of the former are steeper and less embayed. Furthermore, the Teras and Otates faults separate bedrock from internally unfaulted basin fill, whereas the Pitáycachi fault displaces alluvial units by up to 45 m (Bull and Pearthree, 1988). Faults of the Great Basin and southern Basin and Range province that separate bedrock from internally unfaulted basin fill have typically vertical slip rates of at least 0.1 mm/yr, whereas faults that displace alluvium have typically vertical slip rates of 0.01 mm/yr (dePolo and Anderson, 2000).

A rough estimate of the recurrence intervals of these faults can be obtained from their estimated net geologic slip rates and their maximum vertical displacements in the 1887 earthquake; these values are 37 k.y. for the Otates fault, 26 k.y. for the Teras fault, and 27 k.y. for the Pitáycachi fault. These estimates are within the range of recurrence intervals documented for faults of the southern Basin and Range and the Río Grande rift (10–100 k.y.) (Menges and Pearthree, 1989; Machette, 1998). Considering the decrease in the long-term slip rates with time, they are likely to be lower bounds for the Quaternary recurrence intervals of these faults.

The change in Coulomb failure stress caused by the rupture of individual segments of a fault zone may advance or delay the rupture of adjacent segments (King *et al.,* 1994). This suggests that the various segments of the fault zone on the western edge of the Sierra Madre Occidental plateau (Fig. 2) may have failed in the past in segment combinations that are different from the one that ruptured in 1887 (Pitáycachi–Teras–Otates), which probably results in major fluctuations of the recurrence intervals for the individual fault segments.

Distribution of Seismicity

We compiled the seismicity in the epicentral region of the 1887 Sonora earthquake (Fig. 2) from the catalog by DuBois *et al.* (1982), the epicenters relocated by Wallace *et al.* (1988) and Wallace and Pearthree (1989), the macroseismic data reported by Suter (2001), the composite catalog of the United States National Geophysical Data Center, the Preliminary Determination of Epicenters (PDE) catalog of the United States Geological Survey, the catalog of the International Seismological Centre, and the microseismicity study by Natali and Sbar (1982). The distribution of seismicity shows three clusters, which we describe in the following paragraphs.

Most of the seismicity occurs near the 1887 surface rupture and is concentrated at its northern end and in the step-overs between the three rupture segments (Fig. 2). This is especially the case for the well-located microearthquakes. These events, which are marked by closed circles in Figure 2, occurred at a depth shallower than 15 km and have horizontal location errors smaller than 5 km (Natali and Sbar, 1982). They can be interpreted as aftershocks of the 1887 earthquake and explained by an increase of static Coulomb stress (discussed subsequently) at the tips of the individual rupture segments (see Fig. 3). Circumstantial evidence suggests that the horizontal uncertainties of other epicenter locations may also be small: a cluster formed by two low-quality microearthquakes and one PDE event is located exactly in the step-over between the Teras and Otates segments (B and C in Fig. 2), even though the 1887 rupture of this region was not defined at the time when these events were located. The second-largest historical earthquake of this region, the 26 May 1907 M_I 5.2 Colonia Morelos event (Suter, 2001), originated in the step-over between the Pitáycachi and Teras segments of the 1887 rupture (A and B in Fig. 2). Composite focal mechanisms for well-located microearthquakes (Natali and Sbar, 1982) suggest a minor right-lateral strike-slip component near the northern tip and normal dip-slip near the southern tip of the Pitáycachi rupture segment (Fig. 2).

A second cluster, north–south oriented and 30–40 km long, is located east of Fronteras (Fig. 2) and can clearly be separated from the seismicity on the 1887 rupture. These earthquakes, which occurred during 1987–1989, were relocated by Wallace *et al.* (1988) and Wallace and Pearthree (1989). For the largest of these events, which took place on 25 May 1989, Wallace and Pearthree (1989) gave a magnitude of 4.2 and estimated the accuracy of its location as ± 4 km in the east–west direction and ± 5 km in the north–south direction. Three of the microearthquakes recorded by Natali and Sbar (1982) and the epicenter of the 7 April 1908 M_I 4.8 Fronteras earthquake (Suter, 2001) also fall close to this cluster (Fig. 2). Coulomb stress modeling (Fig. 3) indicates that this seismicity cluster is located in a region where the 1887 earthquake caused an increase in static shear stress. These earthquakes may have occurred on the west-dipping Basin and Range fault that bounds the Fronteras valley on its eastern side (Fronteras fault). The earthquake cluster has approximately the same length and orientation as the Fronteras fault, which displaces Quaternary rocks (Nakata *et al.,* 1982) and is characterized on satellite imagery by a morphologically prominent scarp of relatively low relief. Furthermore, the focal mechanism for the 25 May 1989 event determined by Wallace and Pearthree (1989) suggests dip slip with a minor left-lateral strike-slip component on the 65° W-dipping nodal plane (Fig. 2). However, the earthquake cluster is located east of the trace of the west-dipping Fronteras fault (Fig. 2). This may be due to a bias in the location of the teleseismically recorded events and the microseismicity because the azimuthal station coverage does not include stations to the west or south. A field study of the Fronteras fault, relocation of these earthquakes based on a better azimuthal station coverage, and a local microseis-

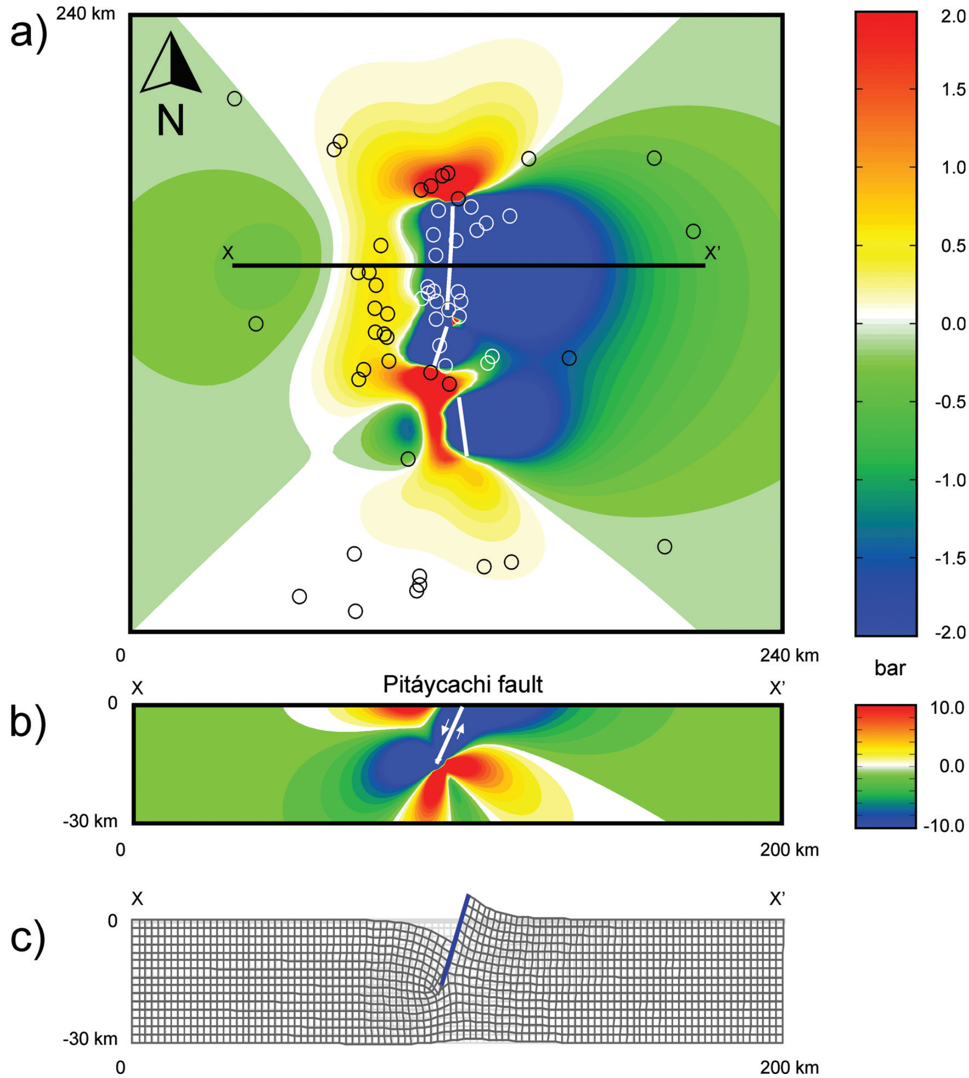

Figure 3. (a) Model of the changes in Coulomb failure stress resulting from the 1887 rupture (white line), at a depth of 7 km on north–south-striking faults with a dip of 75° W. Lobes of stress increase can be observed at the tips of the 1887 rupture segments. A stress buildup is also notable in the region of the Fronteras fault (Fig. 2). The circles represent the epicenters documented in Figure 2. Information on the model parameters is provided in Table 1. (b) Cross section (trace marked in Fig. 3a) of the changes in Coulomb failure stress near the Pitáycachi segment of the 1887 rupture. (c) Same cross section as above showing the calculated coseismic deformation near the Pitáycachi rupture segment. The displacements are exaggerated by a factor of 5000.

micity study are required to evaluate whether the Fronteras fault is active and caused the recorded seismicity.

A third cluster of seismicity exists farther south along the same fault zone, 40–50 km south of the documented southern tip of the 1887 rupture, in the Granados region (Fig. 2). Major events occurred there on 7 May 1913 (Lucero Aja, 1993; Suter, 2001) (I_{max} VIII; M_I 5.0 $\pm$ 0.4) and 20 December 1923 (DuBois *et al.,* 1982; Suter, 2001) (I_{max} IX; M_I 5.7 $\pm$ 0.4). The magnitudes of these events are based on magnitude–intensity relations defined for shallow normal fault earthquakes in the trans-Mexican volcanic belt of central Mexico (Suter *et al.,* 1996); the upper crust can be assumed to have similar attenuation properties in northeastern Sonora and central Mexico since both regions contain Cenozoic volcanic rocks and rift basins. More recently, a series of earthquakes with magnitudes $M_L \leq 4.0$ occurred in the Granados region in 1993. A better definition of the fault network, relocation of the 1993 earthquakes, and microseismicity studies are necessary to understand which of the pronounced faults of the Granados region (Fig. 2) are seismically active. Stress loading by the 1887 rupture on the fault segments near Granados may explain this seismicity cluster (Fig. 3).

Changes in Coulomb Failure Stress Resulting from the 1887 Rupture

Here, we present a model of the change in static Coulomb stress throughout this region resulting from the slip on the three individual segments of the 1887 rupture (Fig. 3a). Our calculations should clarify whether the documented clusters of seismicity (Fig. 2) are related to the changes in Coulomb failure stress. The model could also be helpful for regional seismic hazard evaluations; the locations of stress concentration near the 1887 rupture may indicate faults that are likely to rupture in the future (Stein, 1999). We have applied the Coulomb 2.0 program (Toda *et al.,* 2001), which is designed to calculate displacement, strain, and stress associated with earthquakes (Okada, 1992). The program performs 3D elastic dislocation and a limited number of 2D boundary element calculations of deformation and stress in an elastic half-space. Because we are using a linear theory, we can superimpose the results for the individual rupture segments. The changes in Coulomb failure stress shown in Figure 3 were calculated for north–south-striking faults with a dip of 75° W. The values for the material properties of our model, the regional stress, and the structural parameters of each rupture segment are provided in Table 1.

Our calculations indicate lobes of Coulomb stress increase at the tips of the 1887 rupture segments, especially to the north of the Pitáycachi fault, in the step-over between the Teras and Otates faults, and to the southeast of the Otates fault (Fig. 3a). These stress lobes correlate with the clusters of seismicity documented to the north of the Pitáycachi fault and in the step-over between the Teras and Otates faults (Fig. 2). Furthermore, the cluster of seismicity near Granados (Fig. 2) is located in a region for which we calculated a slight Coulomb failure stress increase of less than 0.2 bar (Fig. 3a).

Models for the change in Coulomb failure stress caused by the rupture of a single normal fault segment (Hodgkinson *et al.,* 1996) would suggest the Fronteras fault and the seismicity cluster near the trace of this fault (Fig. 2) to be located in an area where the 1887 rupture caused a decrease in stress (stress shadow zone), and this seismicity cluster could therefore not be explained by Coulomb stress changes associated with the 1887 earthquake. However, our model for the stress changes resulting from the consecutive rupture of all three individual segments (Fig. 3a) clearly shows a stress buildup of approximately 0.5 bar at a depth of 7 km in the region of this seismicity cluster. A possible explanation for this stress concentration is complex interactions of the stress fields generated by each individual rupture segment (Cowie, 1998; Spyropoulos *et al.,* 1998). Alternatively, the stress concentration near the Fronteras fault may have been induced by coseismic bending of the upper crust (Fig. 3b and c) (Turcotte and Schubert, 1982), which could also explain the stress concentration that appears in our numerical simulation to the east of the Pitáycachi fault at a midcrustal level (Fig. 3b).

Although there is in general a good correlation between the Coulomb failure stress distribution predicted by our model (Fig. 3a) and the documented seismicity distribution (Fig. 2), the model does not explain the microseismicity recorded near the Pitáycachi fault, which is in a zone of pronounced stress drop (Fig. 3a and b). This may be because of the straight-line fault geometry assumed in our model; a better approximation to the less regular trace of the Pitáycachi

Table 1
Parameters Used in the Coulomb Stress Model

Stress Field at a Target Depth of 7 km

Principal Stress	Magnitude (bar)	Orientation
σ_1	2180	vertical
σ_2	2000	north–south
σ_3	1280	east–west

Properties of the Crust

Parameter	Value	Units
Density	2700	kg m^{-3}
Young's modulus	0.8×10^6	bar
Poisson's ratio	0.25	none
Apparent coefficient of friction	0.8	none

Structural Parameters of the Rupture Segments

Segment	Length (km)	Strike (azimuth)	Dip	Average Displacement (m)
Pitáycachi	43.8	2.0°	74° W	2.41
Teras	20.7	11.3°	74° W	1.17
Otates	18.9	−20.2°	74° W	1.58

fault (Fig. 2) may produce local stress concentrations in its vicinity (e.g., Craig, 1996).

Discussion of the Regional Neotectonic Setting

The fault zone along the western margin of the Sierra Madre Occidental plateau has been considered in most studies to be part of the Gulf of California extensional province (e.g., Stock and Hodges, 1989), although in other studies it is considered to be part of the Río Grande rift (e.g., Machette, 1998). This entire region, including the escarpments on the western Gulf of California margin (Fletcher and Munguía, 2000), the Río Grande rift (Aldrich *et al.,* 1986), and our study area, is presently being deformed by east–west extension across north–south-striking high-angle normal faults. The scarps of these faults are evident in regional topographic sections (Fig. 4, traces on Fig. 1). However, extension across the gulf-margin normal faults in Baja California is younger than 11 ± 3 Ma (Fletcher and Munguía, 2000), whereas the fault system along the western margin of the Sierra Madre Occidental initiated about 23 Ma. This system was initially part of an intra-arc setting (Parsons, 1995), and the faults dipped toward the paleotrench associated with the east-dipping subduction zone of the now-extinct Farallon plate.

Several lines of evidence suggest that the faults of our study area are not part of the Río Grande rift. The gravity maps by Keller *et al.* (1990) and Baldridge *et al.* (1995) show in our study area an intermediate-wavelength gravity high that is distinct from the gravity high and associated crustal thinning in the region of the southern Río Grande rift. Furthermore, the Río Grande rift is a relatively symmetrical sag along the axial culmination of the Alvarado topographic ridge (Fig. 4a) and above the underlying zone of crustal thinning (Baldridge *et al.,* 1995), whereas the faults of our study area form, in east–west cross section, a series of half-grabens, with all or most of the graben-bounding faults dipping toward the west (Fig. 4b). This deformation is not located in axial position with respect to the Alvarado ridge, but along its western margin, which coincides here with the western margin of the Sierra Madre Occidental plateau.

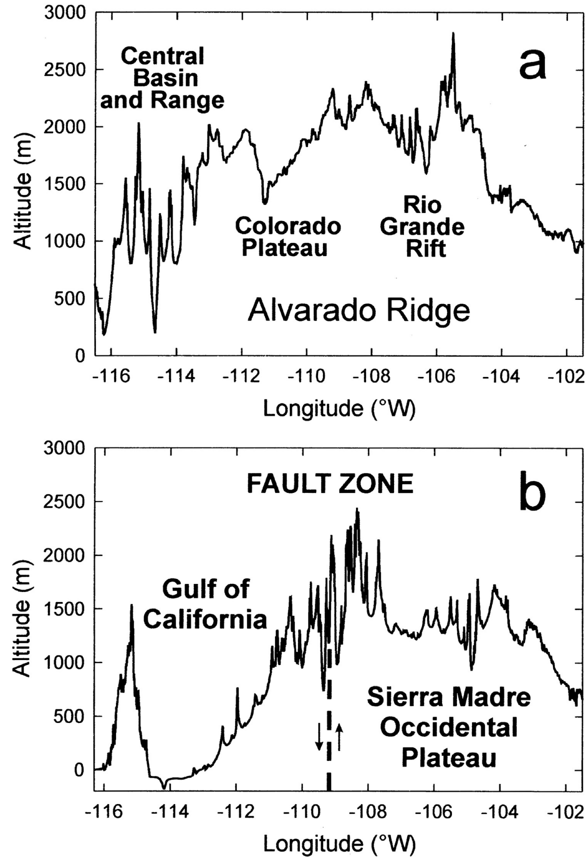

Figure 4. Topographic profiles (a) along 35.6° N and (b) along 30.5° N. The traces of these sections are marked in Figure 1. The fault zone of our study area (dashed line, 1887 rupture) forms, in east–west cross section, a series of half-grabens, with most of the graben-bounding faults dipping toward the west. Contrary to the Río Grande rift, they are not located along the axial culmination of the Alvarado topographic ridge, but along its western margin.

Conclusions

A zone of north–south-striking and west-dipping Basin and Range normal faults forms the western edge of the Sierra Madre Occidental plateau in northeastern Sonora, Mexico. These faults and associated half-grabens extend over a distance of more than 300 km, between the San Bernardino basin in the north and the Sahuaripa basin in the south. A major earthquake occurred in 1887 on three neighboring segments of this fault system; the documented length of the rupture trace measures approximately 100 km, significantly longer than previously reported. The rupture dips about 74° W and is composed (from south to north) of the (1) Otates (length, l = 18.9 km; maximum vertical separation, a = 220 cm; average vertical separation, b = 152 cm), (2) Teras (l = 20.7 km, a = 184 cm, b = 112 cm), and (3) Pitáycachi (l = 43.8 km, a = 487 cm, b = 232 cm) segments.

We compiled seismicity data for this region and compared the distribution of seismicity with our model of the changes in maximum Coulomb shear stress caused by the 1887 rupture. The seismicity is arranged in three clusters. The first cluster is located in the epicentral region of the 1887 earthquake. The events are concentrated near the northern end of the 1887 surface rupture and in the step-overs between the three rupture segments. These events can be interpreted as aftershocks of the 1887 earthquake and coincide with regions of calculated Coulomb failure stress increase at the tips of the individual rupture segments. A second cluster, north–south oriented and 30–40 km long, is located 15–30 km to the west of the events clustered near the 1887 surface rupture trace. The earthquakes of the second cluster seem to be caused by the fault bounding the Fronteras basin on its eastern side. This fault is characterized on satellite images by a morphologically prominent scarp of relatively low relief. Based on our model, the 1887 rupture increased the Coulomb failure stress in this region at a depth of 7 km by about 0.5 bar. A third earthquake cluster is located farther south along the same fault zone, in the Granados region, 40–50 km south of the documented southern tip of the 1887 rupture. The largest events of this cluster occurred on 7 May 1913 (I_{max} VIII) and 20 December 1923 (I_{max} IX). Our model suggests a small buildup of stress (<0.2 bar) on the faults of the Granados region by the 1887 rupture, which may be the reason for these earthquakes.

In cross section, the faults at the western edge of the Sierra Madre Occidental plateau form a staircase pattern of half-grabens, with most of the graben-bounding faults dipping toward the west. These structures are not part of the Río Grande rift as previously assumed. Contrary to the Río Grande rift, they are not located along the axial culmination of the Alvarado topographic ridge, but along its western margin, and do not lie along strike of the rift. Furthermore, the intermediate-wavelength gravity high that exists in our study area is distinct from the gravity high in the region of the southern Río Grande rift.

Acknowledgments

This article has benefited from reviews by Chris Henry, Craig dePolo, John Fletcher, and Randy Keller and discussions with Mike Machette, Raúl Castro, and John Fletcher. Support for this work came from the National Autonomous University of Mexico (UNAM) and the Mexican National Council for Science and Technology (CONACYT, grant G33102-T).

References

Aguilera, J. G. (1888). Estudio de los fenómenos séismicos del 3 de mayo de 1887, *Anales del Ministerio de Fomento de la República Mexicana* **10,** 5–56.

Aldrich, M. J. Jr., C. E. Chapin, and A. W. Laughlin (1986). Stress history and tectonic development of the Rio Grande rift, New Mexico, *J. Geophys. Res.* **91,** 6199–6211.

Baldridge, W. S., G. R. Keller, V. Haak, E. Wendlandt, G. R. Jiracek, and K. H. Olsen (1995). The Rio Grande rift, in *Continental Rifts: Evolution, Structure, Tectonics,* K. H. Olsen (Editor), Elsevier, Amsterdam, 233–275.

Bull, W. B., and P. A. Pearthree (1988). Frequency and size of Quaternary surface ruptures of the Pitaycachi fault, northeastern Sonora, Mexico, *Bull. Seism. Soc. Am.* **78,** 956–978.

Cowie, P. A. (1998). A healing-reloading feedback control on the growth rate of seismogenic faults, *J. Struct. Geol.* **20,** 1075–1087.

Craig, R. R. Jr. (1996). *Mechanics of Materials,* John Wiley and Sons, New York.

dePolo, C. M., and J. G. Anderson (2000). Estimating the slip rates of normal faults in the Great Basin, USA, *Basin Res.* **12,** 227–240.

dePolo, C. M., D. G. Clark, D. B. Slemmons, and A. R. Ramelli (1991). Historical surface faulting in the Basin and Range province, western North America: implications for fault segmentation, *J. Struct. Geol.* **13,** 123–136.

Dixon, T. M., M. Miller, F. Farina, H. Wang, and D. Johnson (2000). Present-day motion of the Sierra Nevada block and some tectonic implications for the Basin and Range province, North American Cordillera, *Tectonics* **19,** 1–24.

Doser, D. I. (1987). The 16 August 1931 Valentine, Texas, earthquake: evidence for normal faulting in west Texas, *Bull. Seism. Soc. Am.* **77,** 2005–2017.

Doser, D. I., and J. Rodríguez (1993). The seismicity of Chihuahua, Mexico, and the 1928 Parral earthquake, *Phys. Earth Planet. Interiors* **78,** 97–104.

DuBois, S. M., A. W. Smith, N. K. Nye, and T. A. Nowak Jr. (1982). Arizona earthquakes, 1776–1980, *State of Arizona, Bureau of Geology and Mineral Technology, Bulletin 193*, 456 pp.

Fernández-Aguirre, M. A., R. Monreal-Saavedra, and A. S. Grijalva-Haro (1993). *Carta geológica de Sonora,* Hermosillo, Sonora, Mexico, Centro de Estudios Superiores del Estado de Sonora (CESUES), scale 1:500,000.

Fletcher, J. M., and L. Munguía (2000). Active continental rifting in southern Baja California, Mexico: implications for plate-motion partitioning and the transition to seafloor spreading in the Gulf of California, *Tectonics* **19,** 1107–1123.

Gans, P. B. (1997). Large-magnitude Oligo-Miocene extension in southern Sonora: implications for the tectonic evolution of northwest Mexico, *Tectonics* **16,** 388–408.

González León, C. M., W. C. Mcintosh, R. Lozano-Santacruz, M. Valencia-Moreno, R. Amaya-Martínez, and J. L. Rodríguez-Castañeda (2000). Cretaceous and Tertiary sedimentary, magmatic, and tectonic evolution of north-central Sonora (Arizpe and Bacanuchi Quadrangles), northwest Mexico, *Geol. Soc. Am. Bull.* **112,** 600–610.

Henry, C. D., and J. J. Aranda-Gómez (2000). Plate interactions control middle-late Miocene proto-Gulf and Basin and Range extension in the southern Basin and Range, *Tectonophysics* **318,** 1–26.

Hodgkinson, K. M., R. S. Stein, and G. C. P. King (1996). The 1954 Rainbow Mountain-Fairview Peak-Dixie Valley earthquakes: a triggered normal faulting sequence, *J. Geophys. Res.* **101,** 25,459–25,471.

Keller, G. R., P. Morgan, and W. R. Seager (1990). Crustal structure, gravity anomalies, and heat flow in the southern Rio Grande rift and their relationship to extensional tectonics, *Tectonophysics* **174,** 21–37.

King, G. C. P., R. S. Stein, and J. Lin (1994). Static stress changes and the triggering of earthquakes, *Bull. Seism. Soc. Am.* **84,** 935–953.

Lucero Aja, C. (1993). Temblores en Sonora, *Historia de Sonora* **84,** 26–28, Dirección General de Documentación y Archivo, Hermosillo, Sonora, Mexico.

Machette, M. N. (1998). Contrasts between short-term and long-term records of seismicity, in *The Río Grande Rift: Important Implications for Seismic-Hazard Assessments in Areas of Slow Extension, Basin and Range Province Seismic-Hazards Summit,* W. R. Lund (Editor), *Utah Geol. Surv. Misc. Publ. 98-2,* 84–95.

McDowell, F. W., J. Roldán-Quintana, and R. Amaya-Martínez (1997). Interrelationship of sedimentary and volcanic deposits associated with Tertiary extension in Sonora, Mexico, *Geol. Soc. Am. Bull.* **109,** 1349–1360.

Menges, C. M., and P. A. Pearthree (1989). Late Cenozoic tectonism in Arizona and its impact on regional landscape evolution, *Arizona Geological Society Digest* **17,** 649–680.

Nakata, J. K., C. M. Wentworth, and M. Machette (1982). Quaternary fault map of the Basin and Range and Rio Grande rift provinces, western United States, *U.S. Geol. Surv. Open-File Rept. 82–579.*

Natali, S. G., and M. L. Sbar (1982). Seismicity in the epicentral region of the 1887 northeastern Sonora earthquake, Mexico, *Bull. Seism. Soc. Am.* **72,** 181–196.

Nieto-Samaniego, A. F., L. Ferrari, S. A. Alaniz-Alvarez, G. Labarthe-Hernández, and J. Rosas-Elguera (1999). Variation of Cenozoic extension and volcanism across the southern Sierra Madre Occidental volcanic province, Mexico, *Geol. Soc. Am. Bull.* **111,** 347–363.

Okada, Y. (1992). Internal deformation due to shear and tensile faults in a half-space, *Bull. Seism. Soc. Am.* **82,** 1018–1040.

Parsons, T. (1995). The Basin and Range Province, in *Continental Rifts: Evolution, Structure, Tectonics,* K. H. Olsen (Editor), Elsevier, Amsterdam, 277–324.

Pearthree, P. A., W. B. Bull, and T. C. Wallace (1990). Geomorphology and Quaternary geology of the Pitaycachi fault, northeastern Sonora, Mexico, *Arizona Geological Survey Special Paper* 7, 124–135.

Spyropoulos, C., C. H. Scholz, and B. E. Shaw (1998). Numerical experiments on transition regimes for the growth of a population of faults, AGU 1998 Spring Meeting, *EOS* (Suppl.), 223.

Stein, R. S. (1999). The role of stress transfer in earthquake occurrence, *Nature* **402,** 605–609.

Stewart, J. H., R. E. Anderson, J. J. Aranda-Gómez, L. S. Beard, G. H. Billingsley, S. M. Cather, J. H. Dilles, R. K. Dokka, J. E. Faulds, L. Ferrari, *et al.* (1998). Map showing Cenozoic tilt domains and associated structural features, western North America, in *Accommodation Zones and Transfer Zones: The Regional Segmentation of the Basin and Range Province,* J. E. Faulds and J. H. Stewart (Editors), Boulder, Colorado, *Geol. Soc. Am. Spec. Pap. 323,* scale: 1:5,000,000.

Stock, J. M., and K. V. Hodges (1989). Pre-Pliocene extension around the Gulf of California and the transfer of Baja California to the Pacific plate, *Tectonics* **8,** 99–115.

Sumner, J. R. (1977). The Sonora earthquake of 1887, *Bull. Seism. Soc. Am.* **67,** 1219–1223.

Suter, M. (1987). Orientational data on the state of stress in northeastern Mexico as inferred from stress-induced borehole elongations, *J. Geophys. Res.* **92,** 2617–2626.

Suter, M. (1991). State of stress and active deformation in Mexico and western Central America, in *Neotectonics of North America,* D. B. Slemmons, E. R. Engdahl, M. D. Zoback, and D. D. Blackwell (Editors), Decade of North American Geology, Decade Map Vol. 1**,** Geological Society of America, Boulder, Colorado, 401–421.

Suter, M. (2001). The historical seismicity of northeastern Sonora and northwestern Chihuahua (28–32° N, 106–111° W), *J. S. Am. Earth Sci.* **14,** 521–532.

Suter, M., M. Carrillo-Martínez, and O. Quintero-Legorreta (1996). Macroseismic study of shallow earthquakes in the central and eastern parts of the trans-Mexican volcanic belt, Mexico, *Bull. Seism. Soc. Am.* **86,** 1952–1963.

Toda, S., R. S. Stein, and G. C. P. King (2001). U.S. Geological Survey Earthquake Hazards Program, Coulomb 2.0 User's Guide, *http://quake.wr.usgs.gov/research/deformation/modeling* (last accessed February 2002).

Turcotte, D. L., and G. Schubert (1982). *Geodynamics, Applications of Continuum Physics to Geological Problems,* John Wiley and Sons, New York.

Wallace, T. C., and P. A. Pearthree (1989). Recent earthquakes in northern Sonora, *Arizona Geology* **19,** no. 3, 6–7.

Wallace, T. C., A. M. Domitrovic, and P. A. Pearthree (1988). Southern Arizona earthquake update, *Arizona Geology* **18,** no. 4, 6–7.

Wells, D. L., and K. J. Coppersmith (1994). New empirical relationships among magnitude, rupture length, rupture width, rupture area, and surface displacement, *Bull. Seism. Soc. Am.* **84,** 974–1002.

Instituto de Geología
Universidad Nacional Autónoma de México (UNAM)
Estación Regional del Noroeste
Apartado Postal 1039
C. P. 83000 Hermosillo, Sonora, Mexico
SuterMax@aol.com
(M.S.)

Departamento de Geología
Centro de Investigación Cientifica y de Educación Superior de Ensenada (CICESE)
Kilómetro 107 Carretera Tijuana-Ensenada
C. P. 22860 Ensenada, Baja California, Mexico
juanc@cicese.mx
(J.C.)

Manuscript received 30 July 2000.